INVESTIGATION OF SUSTAINABLE ALTERNATIVE FUELS FOR THE IRON ORE SINTERING[1]

Jose Adilson de Castro [2]

Abstract
The sintering plant of an integrated steel works is the main supplier of raw materials for the blast furnace process. In conventional sinter plant operation, the fuel commonly used is coke breeze with consumption rate of around 50 kg/t. Regarding to environmental concerns, the sintering produce waste gas and particulates with small concentration of dioxins and furans. This investigation aims to study alternative fuels and smooth operational techniques which minimizes the use of coke breeze and controls the emissions of dioxins and furans. A Mathematical model based on transport equations of momentum, energy and chemical species is used. Biomasses and pre-reduced waste materials are tested as raw materials. Partial recirculation of the outlet gas is proposed as an effective technique to reduce environmental load. The simulation results for an industrial scale plant facility indicated that up to 50% of the waste gas could be reutilized and decrease the dioxin and furans emissions of about 20%. However, the productivity of the sinter strand decreased and the bed permeability must be increased.
Key words: Multiphase model; Sintering; Biomasses.

ESTUDO DE COMBUSTÍVEIS ALTERNATIVOS SUSTENTÁVEIS PARA A SINTERIZAÇÃO DE MINÉRIO DE FERRO

Resumo
A unidade de sinterização de plantas integradas é a principal suplidora de matérias-primas para a produção de gusa em altos-fornos. A operação da sinterização convencional é baseada em finos de coque com um consumo específico em torno de 50 kg/t de sinter. Com relação a aspectos ambientais, a unidade de sinterização produz gases, particulados e pequenas concentrações de compostos policlorados aromáticos como dioxinas e furanos. Neste estudo objetiva-se simular a utilização de combustíveis alternativos com operações estáveis que minimizem o uso de finos de coque e emissões de dioxinas e furanos. O modelo multifásico baseado em equações de transportes de momentum, energia e espécie química foi utilizado e considera os mecanismos das principais reações e transformações de fases que ocorrem no interior do leito de sinterização. Recirculação parcial do gás de exaustão, uso intensivo de biomassa e material pré-reduzido são técnicas propostas visando diminuir o impacto ambiental. Resultados da simulação indicaram que até 50% do gás pode ser utilizado com redução de emissões de dioxinas e furanos, entretanto, a produtividade da sinterização diminui e foi necessário aumentar a permeabilidade do leito.
Palavras-chave: Modelo multifásico; Sinterização; Biomassa.

[1] *Technical contribution to the 7th Japan-Brazil Symposium on Dust Processing-Energy-Environment in Metallurgical Industries and 1st International Seminar on Self-reducing and Cold Bold Agglomeration, September 8-10 2008, São Paulo City – São Paulo State – Brazil*

[2] *Ph.D. Prof. Federal Fluminense University-Post Graduate Program on Metallurgical Engineering – Mechanical Engineering Department – Volta Redonda-RJ- Brazil*

1 INTRODUCTION

In the integrated steel works the sinter plant facilities plays important role furnishing raw materials for the blast furnace and recycling waste materials produced in the subsequent steps of the steel production chain. The sintering process takes place in a moving strand where a mixture of iron ore (sinter feed), fine coke(coke breeze), limestone and water is continuously charged to form a thick bed of approximately 40-80 cm. Along the first meters of the strand the charge is ignited by burners and the fuel combustion propagate the sinter front. The hot gas, generated by the combustion of natural gas with air, is then sucked in through the packed bed from the wind boxes placed below the grate. Figure 1 shows the unit operations involved in the sinter production, such as blending and homogenization, cooling and power production. The process is complex and involves various physical and chemical phenomena such as heat, mass and momentum transfer. These phenomena take place simultaneously increasing considerably the complexity of process analysis and control. The raw materials used can vary to a wide extent, from iron ore to dust recycling. The combustion of fines coke begins at the top of the layers, and as it moves, a relative narrow band of ignition zone moves down through the bed. Several chemical reactions and phase transformations take place within the bed, the materials partially melt when the local temperature reaches the melting temperature and as it moves and exchange heat with the cooling gas, the solidification process occurs. The partial melting and diffusion within the materials promotes the particle agglomeration forming a continuous porous sinter cake. In general, the hot gas produced during sintering can also be re-circulated for better thermal efficiency and environmental savings. Several attempts have been made aiming to predict the final properties of the sinter product. One of the most important parameter is the size distribution which influences strongly the sinter performance within the blast furnace. Waters at al.,[1] developed a mathematical model to predict the final size distribution of the sinter, however, as they pointed out, the model did not considered the kinetics of the sintering phenomena, which strongly affect the final size distribution. Kasai et al.,[2] investigated the influence of the sinter structure into the macroscopic sinter properties. A theoretical explanation of the sintering mechanism and particles interaction were carried out to clarify the bonding forces. They concluded that the void fraction and specific surface area are the main parameters influencing the cake strength. They also concluded that the significant driving forces of structural changes in the sinter cake are compressive and capillary ones. Akiyama et al.[3] investigated the heat transfer properties under the sinter bed conditions and established empirical correlations for the material conductivity. However, there are few comprehensive mathematical models describing the sintering process in an industrial machine such as the usual Dwight-Lloyd. Mitterlehner et al.[4] presented a 1-D mathematical model of the sinter strand focusing on the progression speed of the sintering front. Nath et al.[5] after Cumming et al.[6] developed a 2-D mathematical model based on transport equations, however, their analysis were restricted to a few chemical reactions and the rate of phase transformations were simplified. A more detailed multiphase model has been developed by Castro et al.[7] which has been continuously updated.[8] Therefore, a comprehensive mathematical model able to describe the chemical reactions coupled with momentum, energy and species transport has yet to be continuously improved and applied to simulate the industrial scale of the sintering machine. Moreover, the massive industrial processes using fuels are claimed to reduce all kinds of emissions. Aiming at the investigation of

successfully technologies able to reduce gaseous and particulate emissions, precise models able to predict and indicate optimum operational conditions has to be developed. In the present work, a 3-dimensional mathematical model of the sinter strand is presented based on the multiphase multi-component concept and detailed interactions between the gas and solid phases are addressed. Within the model framework are considered the following phenomena: a) dynamic interaction of the gas mixture with the solids; b) overall heat transfer of all phases; c) vaporization and condensation of water; d) decomposition of carbonates; e) reduction and oxidation of the iron bearing materials; f) fuel combustion and gasification; g) shrinkage of the packed bed; h) partial melt-solidification of the solids and i) phase changes. In this investigation the actual sinter process is simulated and compared with industrial data. Afterwards the influence of the fuel quality is analyzed and other alternative fuels such anthracite and biomasses are tested in order to indicate rational use of natural resources and develop cleaner industrial processes. In addition, alternative recycling technologies are simulated aiming at developing environmentally cleaner operation with low dioxin and furans formation.

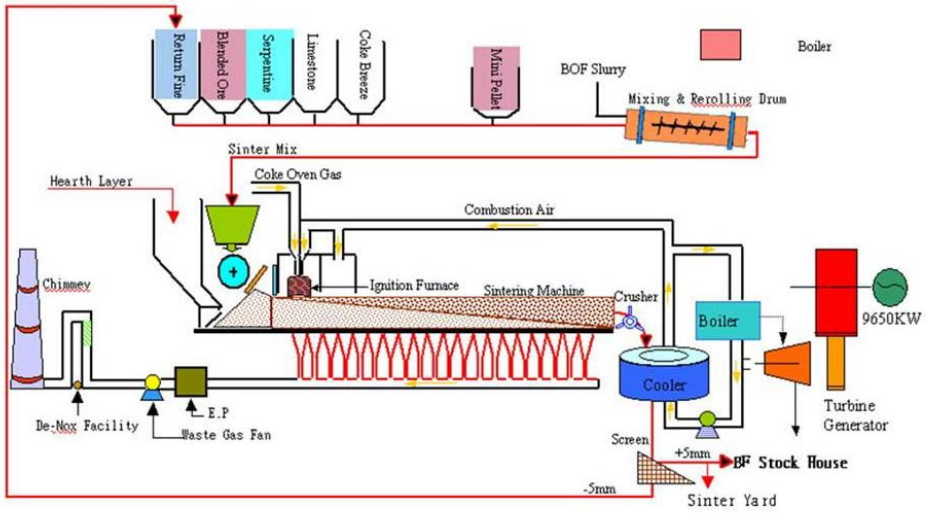

Figure 1. Sinter plant layout and facilities.

Figure 2 illustrates a representative volume of the sinter strand assuming that multiple phases and multiple component coexists exchanging mass momentum and energy. In this work, the multiphase concept is used to model the phenomena within the sinter bed.

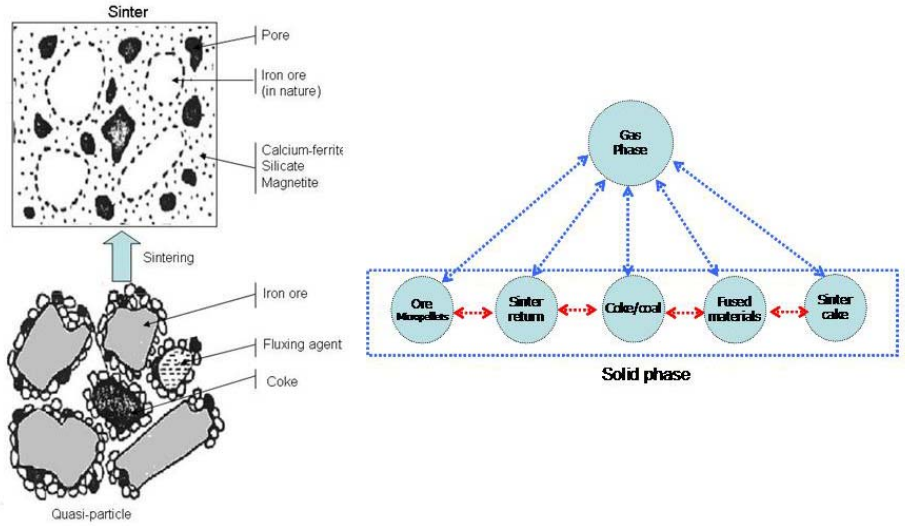

a) Sintering Mechanism b) Multiphase multicomponent concept

Figure 2. Sintering mechanism within the multiphase multicomponent framework concept.

2 METHODOLOGY

2.1 Model Concepts

This model focused on the sinter strand where a representative volume can be visualized as in Figure 2. Within a control volume the solid particles and gas exist at the same time and interacts with one another. In order to model this process, the concept of multiphase and multi-component is assumed. The multiphase principle considers that momentum, energy and chemical species are exchanged among the phases and the rates of transfer are modeled by semi-empirical correlations. In this work, a two phase system is modeled where the solid phase is regarded as a mixture of solid particles having their own properties. In this framework, the solid phase behaves like a non-uniform porous media and the mixture rules are applied to account for the individual contribution of each solid component pondered by their volume fraction. The gas occupies the solid phase porosities and Eq. (1) reads on a continuum approach basis.

$$\varepsilon_s + \varepsilon_g = 1 \tag{1}$$

$$\varepsilon_s = \sum_{m=1}^{m=ncomponents} f_m \tag{2}$$

2.2 Transport Equations

The transport equations for momentum, energy and chemical species for gas and solid phases are presented through eq. 3-6: In table 1 is listed the variables and symbols used in this modeling.[8-12] Table 2 shows detailed chemical species of each phase.[9-12]

Momentum equations:

$$\frac{\partial\left(\rho_i \varepsilon_i u_j\right)}{\partial t} + div\left(\rho_i \varepsilon_i \vec{U}_i u_j\right) = div\left[\varepsilon_i \mu_i grad\left(u_j\right)\right] - grad\left(P_i\right) + F_k^i \tag{3}$$

Continuity:

$$\frac{\partial(\rho_i \varepsilon_i)}{\partial t} + div\left(\rho_i \varepsilon_i \vec{U}_i\right) = \sum_{l=1}^{nreacts} R_l^i \tag{4}$$

Energy:

$$\frac{\partial(\rho_i \varepsilon_i h_i)}{\partial t} + div\left(\rho_i \varepsilon_i \vec{U}_i h_i\right) = div\left[\varepsilon_i \frac{k_i}{C_{p,i}} grad\ (h_i)\right] + E_k^i + \sum_{l=1}^{nreacts} R_l \Delta h_l \tag{5}$$

Chemical species:

$$\frac{\partial(\varepsilon_i \rho_i \phi_{i,ispec})}{\partial t} + div\left(\varepsilon_i \rho_i \vec{U}_i \phi_{i,ispec}\right) = div\left[\varepsilon_i \frac{D_{ispec}^i}{\varepsilon_i \rho_i} grad\left(\phi_{i,ispec}\right)\right] + \sum_{l=1}^{nreacts} M_{ispec} R_l \tag{6}$$

Table 1 Variables and subscripts used in the mathematical formulation

A_{i-k}	Specific phase contact area of the bed [m^2/m^3]		**Subscript**
$\dot{E}_k^i$	Rate of energy exchanged between gas and solid phases (kW)	g	Gas phase
f_m	Volume fraction of solid components (-)	s	Solid phase
F_k^i	Momentum transfer from gas phase to solid phase (N/m^3)	i,k	Index for phase indicator
h_{i-k}	Overall heat transfer coefficient between gas and solid (W/m^2 K)	j	Index for phase velocity components
k_g	Thermal conductivity of gas phase (W/mK)	l	Index for chemical reactions
Pr_g	Prandtl number relating to the gas phase(-)	m	Index to account for phase component

Table 2 Momentum, energy and chemical species for modeling the sintering process

Equations of the gas phase			
Gas	Momentum	$u_{1,g}$, $u_{2,g}$, $u_{3,g}$, P_g, ε_g	
	Energy	h_g	
	Chemical Species	N_2, O_2, CO,CO_2, H_2O, H_2, SiO, SO_2, CH_4, C_2H_6, C_3H_8, C_4H_{10}, dioxin, furan, chrorobenzene	
Equations of the solid phase			
Solid	Momentum	$u_{1,s}$, $u_{2,s}$, $u_{3,s}$, P_s, ε_s	
	Energy	h_s	
	Chemical Species	Coke breeze	C,Volatiles, H_2O, Al_2O_3, SiO_2, MnO, MgO, CaO, FeS, P_2O_5, K_2O, Na_2O, S_2
		Iron ore	Fe_2O_3, Fe_3O_4, FeO, Fe, H_2O, Al_2O_3, SiO_2, MnO, MgO, CaO, FeS, P_2O_5, K_2O, Na_2O
		Return Sinter (bed)	Fe_2O_3, Fe_3O_4, FeO, Fe, H_2O, Al_2O_3, SiO_2, MnO, MgO, CaO, FeS, P_2O_5, K_2O, Na_2O
		Fused Materials	Fe_2O_3, Fe_3O_4, FeO, Fe, H_2O, Al_2O_3, SiO_2, MnO, MgO, CaO, FeS, P_2O_5, K_2O, Na_2O, CaO.Fe3O4, Al2O3.MgO
		Fluxing agent	CaO, H_2O, Al_2O_3, SiO_2, MnO, MgO, TiO_2
		Sinter cake	Fe_2O_3, Fe_3O_4, FeO, Fe, H_2O, Al_2O_3, SiO_2, MnO, MgO, CaO, FeS, P_2O_5, K_2O, Na_2O, CaO.Fe3O4, Al2O3.MgO, dioxin, furan

2.3 Boundary Conditions

The boundary conditions applied to the set of differential conservation equations of the model are of the inlet and outlet type for the gas phase at the top and the bottom faces, respectively. The energy equation uses as inlet boundary condition the average inflow temperature and at the outlet is assumed no temperature gradient. The inlet composition of the solid phase is specified together with solid temperature. For the velocity field, the gas is suctioned and the pressure gradient is used to specify the inlet flow rate at the top surface. The remained boundaries are of symmetry type, where no flux is assumed, except for the temperature field where an effective heat transfer coefficient is specified. Figure 3 shows an insight of the sintering bed evidencing the cooling, preheating, reduction, re-oxidation and combustion zones.

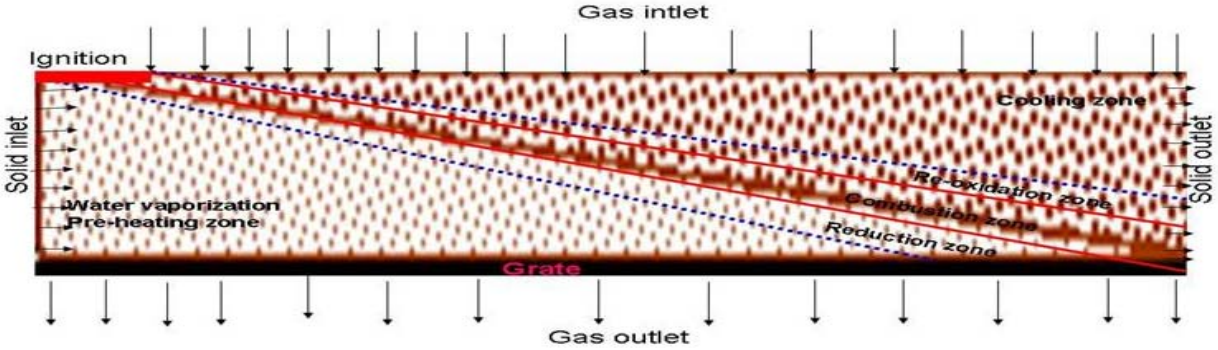

Figure 3 Boundary conditions applied to the sinter bed region

2.4 Source Terms

The interactions between the solid and gas phase is represented though the source terms of each equation. The source terms are due to external forces, interfaces interactions, chemical reactions and phase transformations. This section describes the sub-models used for each of these phenomena

Momentum:

$$F_m = 150\mu_g \frac{1}{\left|\vec{U_g} - \vec{U_s}\right|}\left(\frac{\varepsilon_m}{(1-\varepsilon_m)\, d_m \varphi_m}\right)^2 + 1.75\rho_g \left(\frac{\varepsilon_m}{(1-\varepsilon_m)\, d_m \varphi_m}\right) \tag{7}$$

$$F_g^s = -F_s^g = \left[\sum_m f_m F_m\right]\left|\vec{U}_g - \vec{U}_s\right|\left(\vec{U}_g - \vec{U}_s\right) \tag{8}$$

Heat transfer:

The inter-phase heat transfer considers a local effective coefficient which takes into considerations the combined effect of convection and radiation within the packed bed.[3] In addition, eq. (11) is used to calculate the volumetric available surface to heat transfer.[9-12]

$$\dot{E}_g^s = -\dot{E}_s^g = h_{g-s} A_{s-g} \left[T_s - T_g \right] \tag{9}$$

$$h_{s-g} = \frac{k_g}{d_s} \left[2.0 + 0.39 \left(Re_{g-s} \right)^{0.5} \left(Pr_g \right)^{1/3} \right] \tag{10}$$

$$A_{s-g} = \sum_m \left(f_m \frac{6\varepsilon_m}{d_m \varphi_m} \right) \tag{11}$$

Chemical reactions:

The model takes into consideration major chemical reactions and phase transformations. Additionally, in this work a mechanism of dioxins and furans formation are addressed. Table 3 shows the chemical reactions, phase transformations and dioxins/Furans considered in this model. The rate equations for chemical reactions, phase transformation and PCDDs and PCDFs are found elsewhere.[8-12]

The PCCD/Fs, are groups of chlorinated tricyclic aromatic compounds where different degrees and compounds of chlorination on the aromatic ring structures can occur forming 75 PCDD and 135 PCDF isomers. In the environment PCD/Fs are found in traces quantities as mixture of the isomers and often referred to as “dioxins”. It is believed that some isomers of dioxin may have carcinogenic and mutagenic effects. Regarding to industrial process, our concern is due to, in high temperature process of sintering iron ore, carbon source materials such as coal and biomasses are used as heat supplier. In the sinter process of iron ore some small amount of dioxins and furans are formed and represent a dangerous contaminant for humans. Although it is well known that PCCD/Fs may be formed in many combustion processes, it is not yet possible completely understand the mechanism of formation, because the chemical reactions are very complex involving gas and condensed phases[9,13]. Heterogeneous reactions mechanisms have been proposed in order to explain the formation and destruction of the PCCD/Fs.[9,10,13]

In the present work, a kinetic model of PCCD/Fs formation via de novo synthesis is investigated, as presented in table 3. The basic molecule of dioxins and furans are presented in Figure 4, where *α* and *β* are positions occupied by chorine and hydrogen.

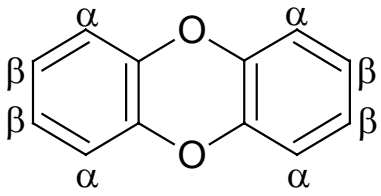

a) Dioxin -PCDDs (Policlorine Dibenzene -p-Dioxin)

$C_{12}O_2H_xCl_{(8-x)}$

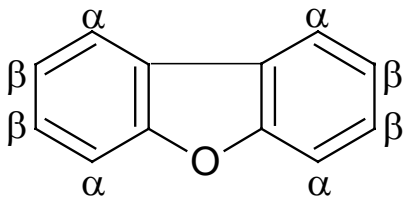

b) Furan-PCDFs (Policlorine Dibenzenefurans)

$C_{12}OH_xCl_{(8-x)}$

Figure 4 Basic structure for dioxin and furan formation

Table 3 Chemical reactions considered in the model

R_i	Chemical Reactions
Reduction by CO	
1_i	$\mathbf{3\,Fe_2O_3}(i)+\mathbf{CO}(g)\rightarrow 2\,\mathbf{Fe_3O_4}(i)+\mathbf{CO_2}(g)$ $(i\rightarrow \text{ore, sin ter, fines, etc})$
2_i	$\frac{\mathbf{w}}{\mathbf{4w-3}}\mathbf{Fe_3O_4}(i)+\mathbf{CO}(g)\rightarrow \frac{3}{4w-3}\mathbf{Fe_wO}(i)+\mathbf{CO_2}(g)$ $(i\rightarrow \text{ore, sin ter, fines, etc})$
3_i	$\mathbf{Fe_wO}(i)+\mathbf{CO}(g)\rightarrow w\,\mathbf{Fe}(i)+\mathbf{CO_2}(g)$ $(i\rightarrow \text{ore, sin ter, fines, etc})$
Reduction by H_2	
4_i	$\mathbf{3\,Fe_2O_3}(i)+\mathbf{H_2}(g)\rightarrow 2\,\mathbf{Fe_3O_4}(i)+\mathbf{H_2O}(g)$
5_i	$\frac{\mathbf{w}}{\mathbf{4w-3}}\mathbf{Fe_3O_4}(i)+\mathbf{H_2}(g)\rightarrow \frac{3}{4w-3}\mathbf{Fe_wO}(i)+\mathbf{H_2O}(g)$
6_i	$\mathbf{Fe_wO}(i)+\mathbf{H_2}(g)\rightarrow w\,\mathbf{Fe}(i)+\mathbf{H_2O}(g)$ $(i\rightarrow \text{ore, sin ter, fines, etc})$
Re-oxidation of solids	
7_i	$\mathbf{w\,Fe}\ (i)+\frac{1}{2}\mathbf{O_2}(g)\rightarrow \mathbf{Fe_wO}(i)$
8_i	$\frac{3}{4w-3}\mathbf{Fe_wO}(i)+\frac{1}{2}\mathbf{O_2}(g)\rightarrow \frac{\mathbf{w}}{\mathbf{4w-3}}\mathbf{Fe_3O_4}(i)$
9_i	$\mathbf{2\,Fe_3O_4}(i)+\mathbf{O_2}(g)\rightarrow 3\,\mathbf{Fe_2O_3}(i)$ $(i\rightarrow \text{ore, sin ter, fines, etc})$
Gasification of carbon	
10_i	$C(i)+\frac{1}{2}\mathbf{O_2}(g)\rightarrow CO(g)$
11_i	$C(i)+\mathbf{O_2}(g)\rightarrow CO_2(g)$
12_i	$C(i)+\mathbf{CO_2}(g)\rightarrow 2CO(g)$
13_i	$C(i)+\mathbf{H_2}O(g)\rightarrow H_2(g)+CO(g)$ $(i\rightarrow \text{coke breeze or coal})$
Gasification of volatiles	
14_i	$\text{Volatiles}(i)+\alpha_1O_2(g)\rightarrow \alpha_2CO_2(g)+\alpha_3H_2O(g)+\alpha_4N_2(g)$
15_i	$\text{Volatiles}(i)+\alpha_5CO_2(g)\rightarrow \alpha_6CO(g)+\alpha_7H_2(g)+\alpha_8N_2(g)$ $(i\rightarrow \text{coke breeze or coal})$
Water gas shift	
16	$CO_2(g)+H_2(g)\rightarrow CO(g)+H_2O(g)$
Phase transformation	
17_i	$H_2O(i)\leftrightarrow H_2O(g)$ $(i\rightarrow \text{ore, sin ter, coke})$
18_i	$CaO(i)\leftrightarrow CaO(l)$
19_i	$MgO(i)\leftrightarrow MgO(l)$
20_i	$MnO(i)\leftrightarrow MnO(l)$
21_i	$Al_2O_3(i)\leftrightarrow Al_2O_3(l)$ $(i\rightarrow \text{ore, sin ter, coke})$
22_i	$CaO(i)+FeO(i)\leftrightarrow (CaO).(FeO)$ $(i\rightarrow \text{ore, sin ter, coke})$
23_i	$2CaO(i)+FeO(i)\leftrightarrow (CaO)_2.(FeO)$ $(i\rightarrow \text{ore, sin ter, coke})$
Dioxin formation	
24_i	$48\,C_{(s)}+2.5O_2+16\,HCl_{(g)}+4\,H_{2(g)}\leftrightarrow C_{12}OH_5Cl_{3(g)}+C_{12}O_2H_5Cl_{3(g)}+$ $+2\,C_6H_3Cl_2OH_{(g)}+2\,C_6H_3Cl_{3(g)}$
25_i	$2\,\left[C_6H_3Cl_2OH_{(s)}\right]\rightarrow C_{12}OH_5Cl_{3(s)}+HCl_{(g)}+H_2O_{(g)}$
26_i	$C_6H_3Cl_2OH_{(s)}+C_6H_3Cl_{3(s)}+0.5O_{2(g)}\rightarrow C_{12}O_2H_5Cl_{3(s)}+2HCl_{(g)}$

2.5 Numerical features

The model equations described above are discretised based on the Finite Volume Method (FVM) where the coupling of velocity and pressure field is done by applying the simple algorithm with staggered covariant velocity components located on the face of the finite volumes. The source terms were linearized and the resulting algebraic equations were iteratively solved based on tri-diagonal matrix line by line

method(ADI). A computational code based on Fortran 90 was implemented and the computational domain was divided into 20x180x10 control volumes. Figure 4 shows the local coordinate system and computational molecule for the finite volume integration of the differential equations. In the finite volume method the general transport equation is integrated over the finite control volume with the volumetric fluxes calculated over the surfaces based on the Gauss theorem with resulting algebraic equations are presented in compact form, eq. (18), where the coefficients accounts for the information carried by the neighbor volumes and estimated by the power law scheme.

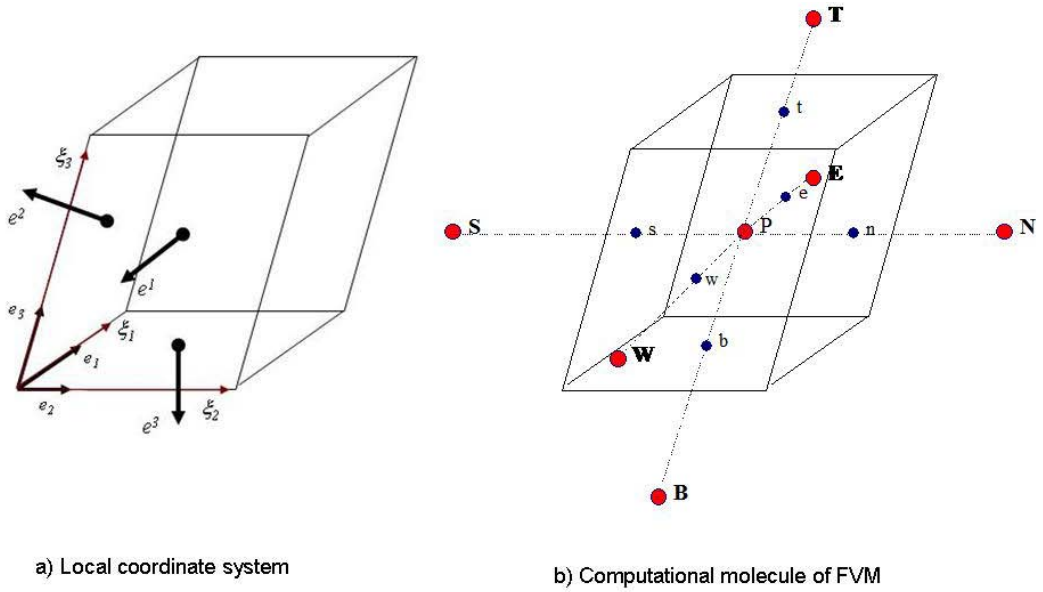

a) Local coordinate system

b) Computational molecule of FVM

Figure 4 Computational molecule and the coordinate system used to discretise the domain into finite volumes

$$\int_{\delta t}\int_{\delta V}\frac{\partial(\rho\varepsilon\phi)}{\partial t}dvdt+\int_{\delta t}\int_{\delta V}\left[div\left(\rho\varepsilon\vec{U}\phi-\varepsilon\Gamma_{\phi}grad(\phi)\right)\right]dvdt=\int_{\delta t}\int_{\delta V}S_{\phi}dvdt \tag{12}$$

$$\int_{\delta t}\int_{\delta V}\frac{\partial(\rho\varepsilon\phi)}{\partial t}dvdt\approx J\frac{\left(\rho\varepsilon\phi_{P}-\rho^{0}\varepsilon^{0}\phi_{P}^{0}\right)}{\Delta t} \tag{13}$$

$$\int_{\delta t}\int_{\delta V}\left[div\left(\rho\varepsilon\vec{U}\phi-\varepsilon\Gamma_{\phi}grad(\phi)\right)\right]dvdt\approx F.A\rangle_{e}-F.A\rangle_{w}+F.A\rangle_{n}-F.A\rangle_{s}+F.A\rangle_{t}-F.A\rangle_{b} \tag{14}$$

$$\int_{\delta t}\int_{\delta V}S_{\phi}dvdt\approx S_{C}+S_{P}\phi_{P} \tag{15}$$

$$F.A\rangle_{e}=\int_{A_e}F.dA=\left(\rho\varepsilon\vec{U}.A^{(1)}\phi-\varepsilon\Gamma A^{(1)}.\nabla\phi\right)\rangle_{A_e}=F^{(1)}\rangle_{e} \tag{16}$$

$$F^{(1)}\rangle_e = \left[\rho\varepsilon U^1 \phi - \varepsilon\Gamma\left(G^{11}\frac{\partial\phi}{\partial\xi^1} + G^{12}\frac{\partial\phi}{\partial\xi^2} + G^{13}\frac{\partial\phi}{\partial\xi^3} \right) \right] \Bigg\rangle_e \tag{17}$$

$$a_P\phi_P = a_W\phi_W + a_E\phi_E + a_B\phi_B + a_T\phi_T + a_S\phi_S + a_N\phi_N + b \tag{18}$$

$$a_P = a_W + a_E + a_B + a_T + a_S + a_N + a_P^0 - S_P \tag{19}$$

$$b = b_{NO} + S_C + a_P^0\phi^0 \tag{20}$$

$$b_{NO} = \left[\Gamma G^{12}\frac{\partial\phi}{\partial\xi^2} + \Gamma G^{13}\frac{\partial\phi}{\partial\xi^3} \right]_w^e + \left[\Gamma G^{21}\frac{\partial\phi}{\partial\xi^1} + \Gamma G^{23}\frac{\partial\phi}{\partial\xi^3} \right]_s^n + \left[\Gamma G^{31}\frac{\partial\phi}{\partial\xi^1} + \Gamma G^{32}\frac{\partial\phi}{\partial\xi^2} \right]_b^t \tag{21}$$

3 RESULTS AND DISCUSSION

This section outlines the calculation results obtained for different fuels and PCDDs/PCDFs emissions. The fuels used in this calculation were coke breeze, anthracite and as biomass charcoal. Table 4 shows the fuels compositions used in this investigation. For the PCDDs/PCDFs investigation the calculations were carried out for coke breeze and charcoal aiming the comparison of these fuels with regarding to PCDDs/PCDFs emissions. Figure 5a shows the effect of fuels into the location of thermal and chemical fronts. The higher temperature pick is observed for coke breeze contrarily indicated by biomass operation. Figure 5b shows the effect of fuel size diameter, however, the volume fraction of the fuel is small compared with the iron bearing solids, which leads to small effect on the thickness of the combustion zone but the temperature pick increased around 40 ^{o}C for coke breeze diameter of 3 mm.

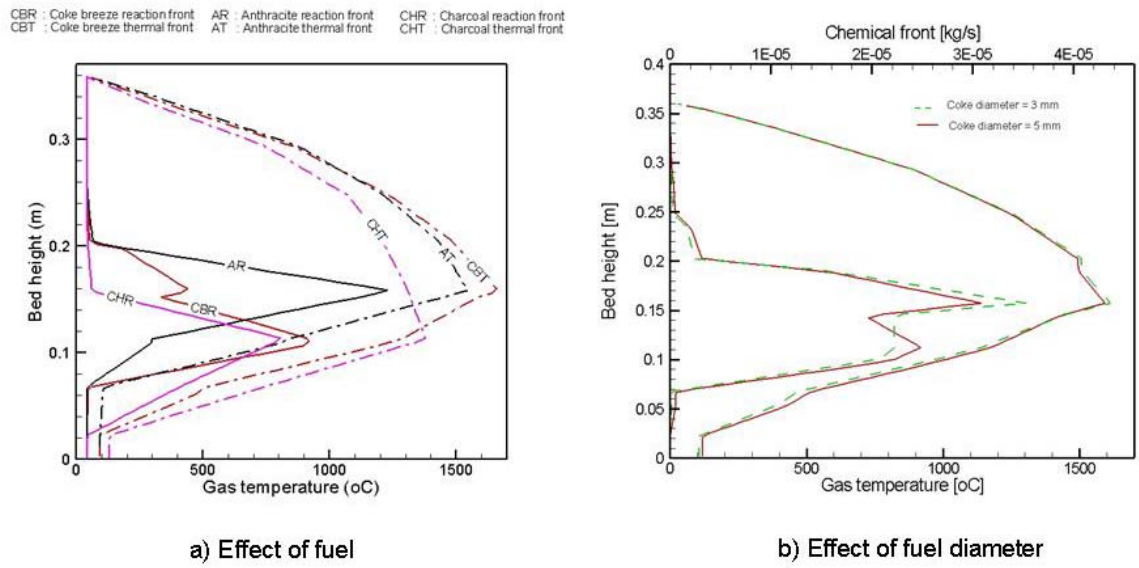

Figure 5 Effects of raw materials on the position and thickness of thermal and chemical fronts

Table 4 Fuels compositions

Elemental analysis (%)	Coke breeze	Anthracite	Charcoal
Fixed carbon	82.59	84.84	70
Volatile matter	-	4.26	25
Ash	9.81	8.90	2
H2O	4.2	2.0	3
Total carbon	85.9	85.66	79.4
Oxygen	4.2	3.72	6.5
Nitrogen	0.8	0.33	2.3
Hydrogen	0.2	0.82	5.4
Phosphorus	NI	NI	0.5
Sulfur	NI	0.45	0.05
Ash			
SiO2	58.9	46.93	31
Al2O3	34.3	41.53	3
Fe2O3	NI	1.8	NI
MnO2	NI	NI	NI
MgO	0.98	1.4	6.5
CaO	1.9	2.2	41

Figure 6 presents the sintering front predictions on the industrial machine used for validate the model. The measured temperature of final position of the sintering front was measured and compared with the model predictions with error norm less than 3% for all calculations of the actual operation, then, these data were used to comparison with other operational practices. Figure 7 shows the effect of temperature distribution of the sinter bed for different fuels. The temperature field of the sintering front for coke breeze is higher and thicker due to higher calorific value, although the combustion kinetics is lower. Therefore, there is compensation when biomass is used due to its higher combustion rates. The result is an enlargement of the sintering zone with lower temperature and higher residence time of the solids in this region. The heat input compensations is done by additional consumption of fuels.

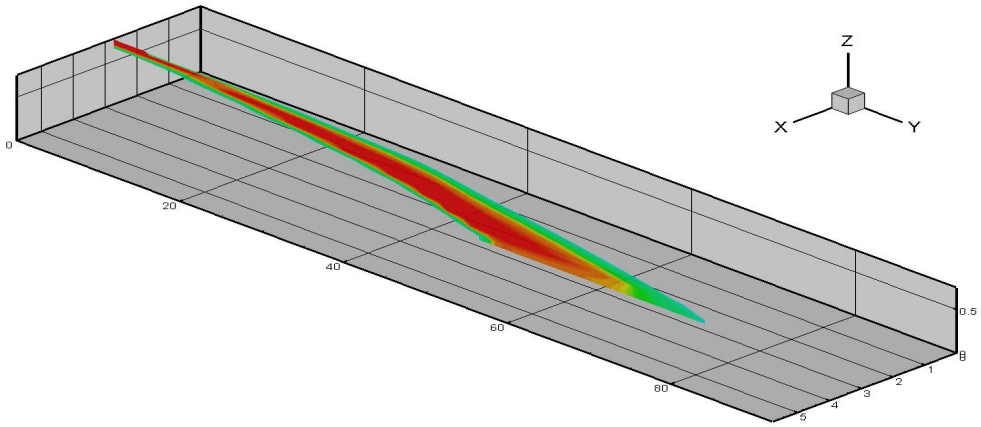

Figure 6 Computed results of sintering front with coke breeze as fuel

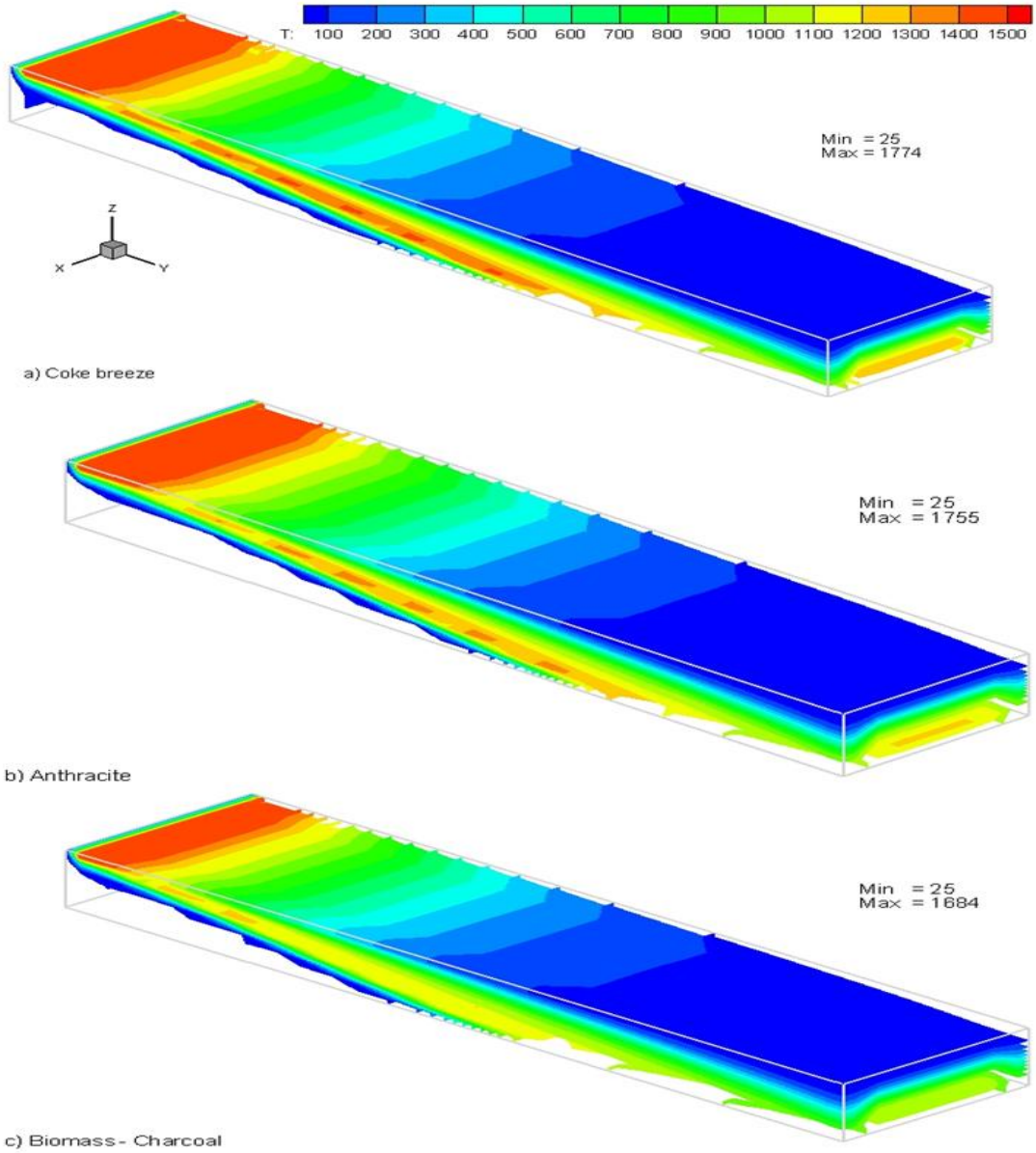

Figure 7 Computed results for coke breeze, anthracite and biomass used as fuel for the sintering process

Figures 8 show the temperature field of the sintering bed. The calculation results indicate smooth operation of the sintering machine with well defined region of heating, reduction, combustion, re-oxidation and cooling. In such conditions the dioxins and furans are generated and destructed inside the bed, as observed in fig. 9 and 10. The model predicts the pattern of PCDDs/PCDFs strongly dependent on the temperature field, but with displacement of temperature range for PCDFs for higher temperature while PCDDs are mainly formed at lower temperatures.

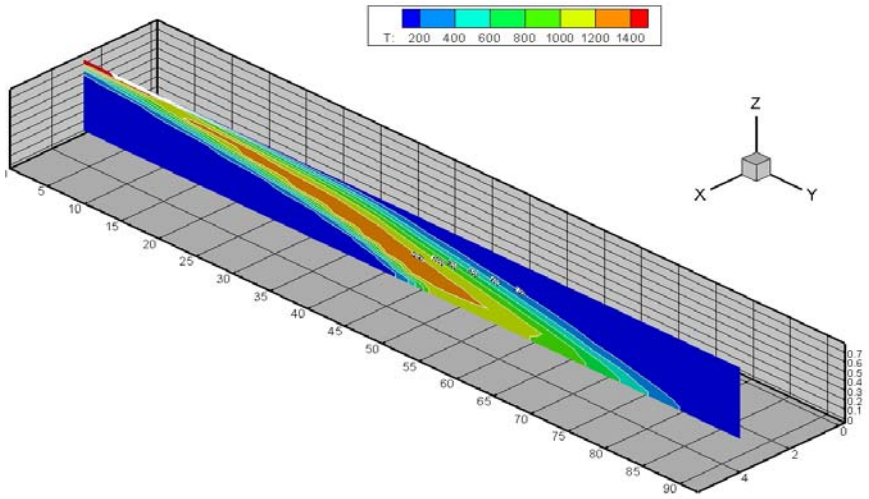

Figure 8 Computed results for coke breeze, anthracite and biomass used as fuel for the sintering process

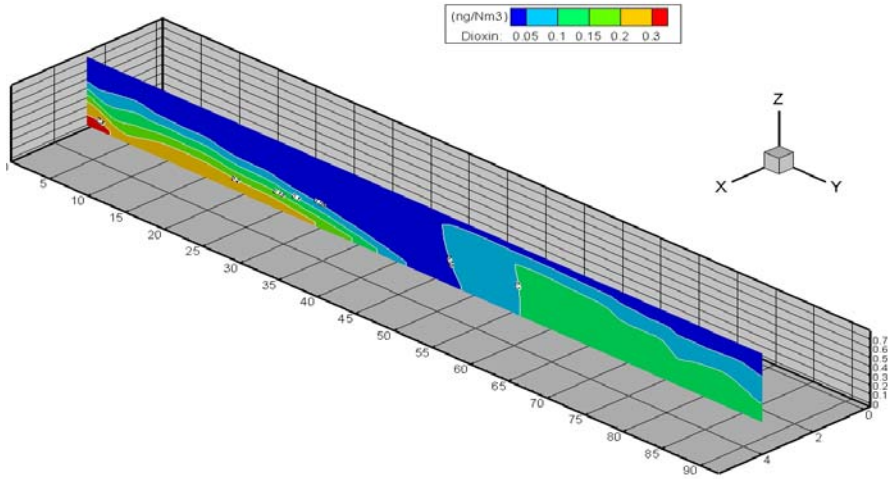

Figure 9 Dioxins distribution within the sintering bed operation based on coke breeze

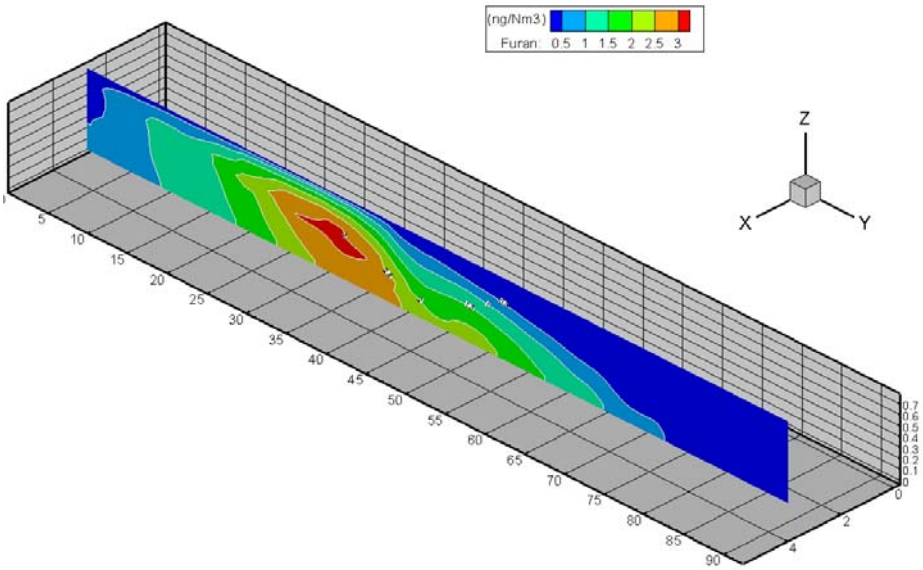

Figure 10 Furans distribution within the industrial sintering bed operation based on coke breeze

The effect of using biomass on the sintering machine is shown in Figure 11 with respect to dioxins and furans emissions. The model predicts lower emissions for charcoal compared with coke breeze. This result is due to mainly the inner temperature distribution within the sintering machine and lower ash content of the charcoal.

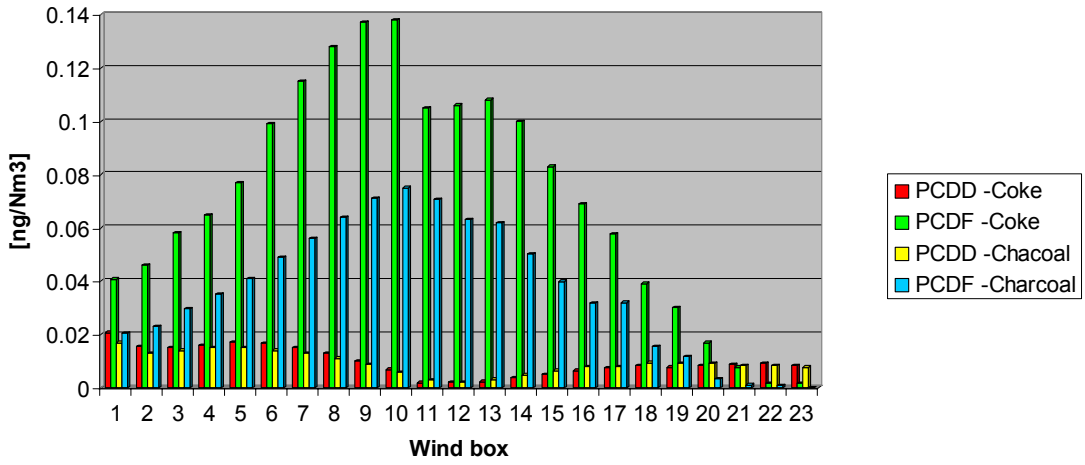

Figure 11 Comparison of dioxins and furans distributions along the wind box of the sintering machine for coke breeze and charcoal

Figure 12 shows the distribution pattern of PCDDs and PCDFs emissions of each wind box when outlet gas recirculation is applied. The central region of the machine shows higher concentrations for PCDFs while PCDDs are concentrated into the initial and final stage of sinter bed. This model, however is able to predict not only global emissions but also the key point in the interior of the sinter bed to be controlled and indicating conditions of low emissions.

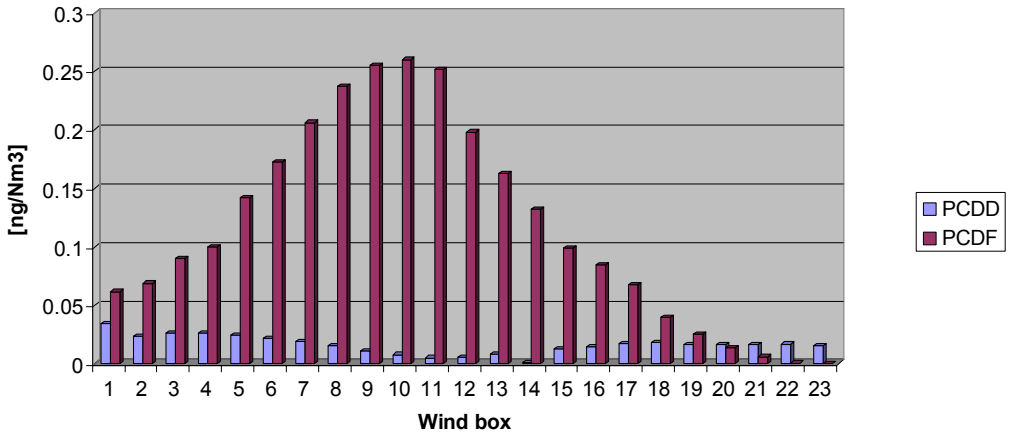

Figure 12 Dioxins and furans distributions along the wind box of the sintering machine using 20% of dust gas recycling

4 CONCLUDING REMARKS

In this work a multi-phase mathematical model has been developed and applied to simulate the sinter plant of an integrated steel industry. The model is based on transport equations of momentum energy and chemical species coupled with chemical reaction of reduction, combustion, oxidation and physical transformation such as melting water evaporation and condensation. The model was used to investigate alternative fuels candidates aiming at increasing the possibility of blending raw materials for using in the industrial scale sintering process. In addition, the model was used to investigate PCDDs and PCDFs emissions. Simulation results indicated that only 100% of biomass is possible, however, possibly sinter strength would decrease considerably due to the lower temperature of the thermal front and consequently small sintering fraction due to liquid phases. With regarding to PCDDs/PCDFs emissions the biomass showed good potential for lower emissions, however, lower temperature gradient near the 450 ^{o}C could be an impediment for such practice. In this investigation, a emission decrease of around 15% was found with biomass compared with coke breeze in spite of increase of fuel rate of approximately 6%.

5 Aknowlegments

The authors thanks to CNPQ and Faperj (Research grant: Yong Scientist of the Rio de Janeiro State – 2007-2009) for the financial support on the development of this project

REFERENCES

1 Waters, A. G. Litster, J.D. and Nicol, S.K. , 1989 “A Mathematical Model for the Multicomponent Sinter Feed”, ISIJ International, Vol. 29, pp. 274-283.
2 Kasai, E. Batcaihan, B. Omori, Y. Sakamota, N. and Kumasaka, A.,1991 “Permeation Characteristics and Void Structure of Iron Ore Sinter Cake”, ISIJ International., Vol. 31, pp. 1286-1291.
3 Akiyama, T. Ohta, H. Takahashi, R. Waseda, O. and Yagi, J. , 1992 “Measurement of Oxide and Porous Modeling of Iron Ore Thermal Conductivity for Dense iron Agglomerates in Stepwise Reduction”, ISIJ International., Vol. 32, pp. 829-837.
4 Mitterlehner, J. Loeffler, G. Winter, F., Hofbauer, H., Schmid, H. Zwittag, E. , Buergler, H. Pammer, O. and Stiansy, H. , 2004 “Modeling and Simulation of Heat Front Propagation in the Iron Ore Sintering Process”, ISIJ International., Vol. 44, pp. 11-20.
5 Nath, N. K. Silva, A.J. and Chakraborti, N. , 1997 “Dynamic Process Modelling of Iron Ore Sintering”, Steel Research, vol 68, pp 285-292.
6 Cumming, M.J. and Thurlby, J. A. , 1990 “ Development in Modelling and Simulation of Iron Ore Sintering”, Ironmaking and Steelmaking, vol 17, pp 245-254.
7 Austin, P.R., Nogami, H. and Yagi, J., 1997, “A Mathematical Model of Four Phase Motion and Heat Transfer in the Blast Furnace”, ISIJ International., Vol. 37, pp. 458-467.
8 Austin, P.R., Nogami, H. and Yagi, J., 1997, “A Mathematical Model for Blast Furnace Reaction Analysis Based on the Four Fluid Model”, ISIJ International, Vol. 37, pp. 748-755.

9 Castro, J.A., Nogami, H. and Yagi, J., 2006, “Industrial Process Simulation Based on Multiphase Mathematical Model: Application to Predict the Sinter Plant Operation” Proceedings of the 11th Brazilian Congress of Thermal Sciences and Engineering -- ENCIT 2006, Curitiba, Brazil, pp. 1-10
10 Castro, J.A. Silva, A.J. , Nogami, H. e Yagi, J. , 2005, “ Tecnologia em Metalurgia e Materiais, Vol 2, pp 45-52.
11 Castro, J.A., Nogami, H. and Yagi, J., 2002, “Three-dimensional Multiphase Mathematical Modeling of the Blast Furnace Based on the Multifluid Model”, ISIJ International., Vol. 42, pp. 44-52.
12 Castro, J.A, 2001, “A multi-dimensional transient mathematical model of the blast furnace based on the multi-fluid model”. Ph.D thesis, IMRAM – Institute for multidisciplinary research for advanced materials – Tohoku University – Japan
13 Harjanto, S., Kasai,E., Terui, T. and Nakamura, T. “Behavior of Dioxin During Thermal Remediation in the Zone Combustion Process, 2002, Chemosphere, vol. 47, pp.687-693.